npj | climate and atmospheric science

Article

Published in partnership with CECCR at King Abdulaziz University

https://doi.org/10.1038/s41612-025-01020-0

Stratospheric ozone depletion has contributed to the recent tropical La Niña-like cooling pattern

Yue Dong[1] ✉, Lorenzo M. Polvani[2,3], Yen-Ting Hwang[4] & Mark R. England[5]

Despite the continuous global warming, over the past several decades, the tropical East Pacific has experienced a cooling trend whose origin remains an area of active research. Mounting evidence has linked tropical sea-surface temperature (SST) patterns to changes in the Southern Ocean via remote teleconnections. Using a fully-coupled global climate model, we demonstrate that stratospheric ozone depletion can produce a La Niña-like tropical SST trend pattern resembling recent observations. This tropical response initially arises from mid-latitude ocean adjustments to ozone-driven surface wind anomalies, which then enhance in the tropics via positive cloud feedback and wind-evaporation-SST feedback. Our finding suggests that the observed La Niña-like tropical SST trend pattern may have been, in part, caused by the formation of the ozone hole in the late 20th century. It also implies that ozone recovery in the coming decades will likely contribute to a future weakening or reversal of the observed tropical SST trends.

Despite widespread warming on a global scale, the observed sea-surface temperature (SST) trend pattern over recent decades features a remarkable cooling in the tropical East Pacific[1,2] (EP; Fig. 1a–c). This La Niña-like tropical SST trend pattern has been linked to a broad range of observed climate changes, including the anomalously low value of effective climate sensitivity derived from observations[3,4], the strengthening of the Walker Circulation[5,6], and the persistent drying trend in the American Southwest[7,8]. Climate models, on the other hand, tend to project an El Niño-like warming pattern – the opposite of the one recently observed – to emerge in the future under rising greenhouse gas (GHG) forcing[1,9]. The fact that models generally fail to reproduce the observed La Niña-like historical warming pattern adds considerable uncertainty to the model projections.

Despite its importance, the causes of the observed tropical SST trend pattern remain elusive. While model large ensembles suggest an important role of internal variability in modulating the decadal changes in tropical SST patterns[10,11], single forcing simulations also reveal contributions from anthropogenic aerosol forcing[12–14] and GHG forcing[15]. For example, increased aerosol emissions could drive large-scale atmospheric circulation changes featuring enhanced northern hemisphere tropical trader winds or slow timescale tropical ocean adjustment that both lead to tropical cooling[12–14]. CO_2 increase may also cause a transient tropical cooling response driven by tropical eastern Pacific upwelling – the so-called ocean thermostat mechanism[15,16]. Beyond mechanisms involving tropical local processes, mounting evidence is pointing to the role of the remote impact from the Southern Ocean (SO) via teleconnections. A La Niña-like pattern of tropical SST response has been shown in a hierarchy of model simulations with idealized[17,18] or realistic SO cooling[19,20]. Similar results are found in experiments with SO non-thermal forcings (i.e., other than SST and surface heat fluxes), notably Antarctic wind anomalies[21] and Antarctic ice-sheet melting[22], confirming the SO remote impacts on the tropics.

Building on the modeling evidence, a recent paper[23], has proposed that the observed La Niña-like tropical SST pattern may have arisen from the formation of the Antarctic ozone hole via the Southern Annular Model (SAM) and its impact on surface winds and SO SST. Indeed, the SAM–associated with the strengthening of surface westerlies over the SO[24] – has become more positive in the late 20th century[25,26], largely due to stratospheric ozone depletion[27,28]. Using observational reanalysis, that study[23] noted that the monthly SST anomalies associated with the SAM feature a cooling response in the SO and tropical EP, and hypothesized that stratospheric ozone depletion could have contributed to the formation of the observed La Niña-like tropical pattern through the SO-tropics teleconnections.

That hypothesis, however, is open to several questions in the proposed linkage between the ozone hole and tropical cooling. First, the observed

[1]Department of Atmospheric and Oceanic Sciences, University of California Los Angeles, Los Angeles, CA, USA. [2]Lamont-Doherty Earth Observatory, Columbia University, Palisades, NY, USA. [3]Department of Applied Physics and Applied Mathematics, Columbia University, New York, NY, USA. [4]Department of Atmospheric Sciences, National Taiwan University, Taipei, Taiwan, ROC. [5]Department of Mathematics and Statistics, University of Exeter, Exeter, UK.
✉e-mail: ydong@atmos.ucla.edu

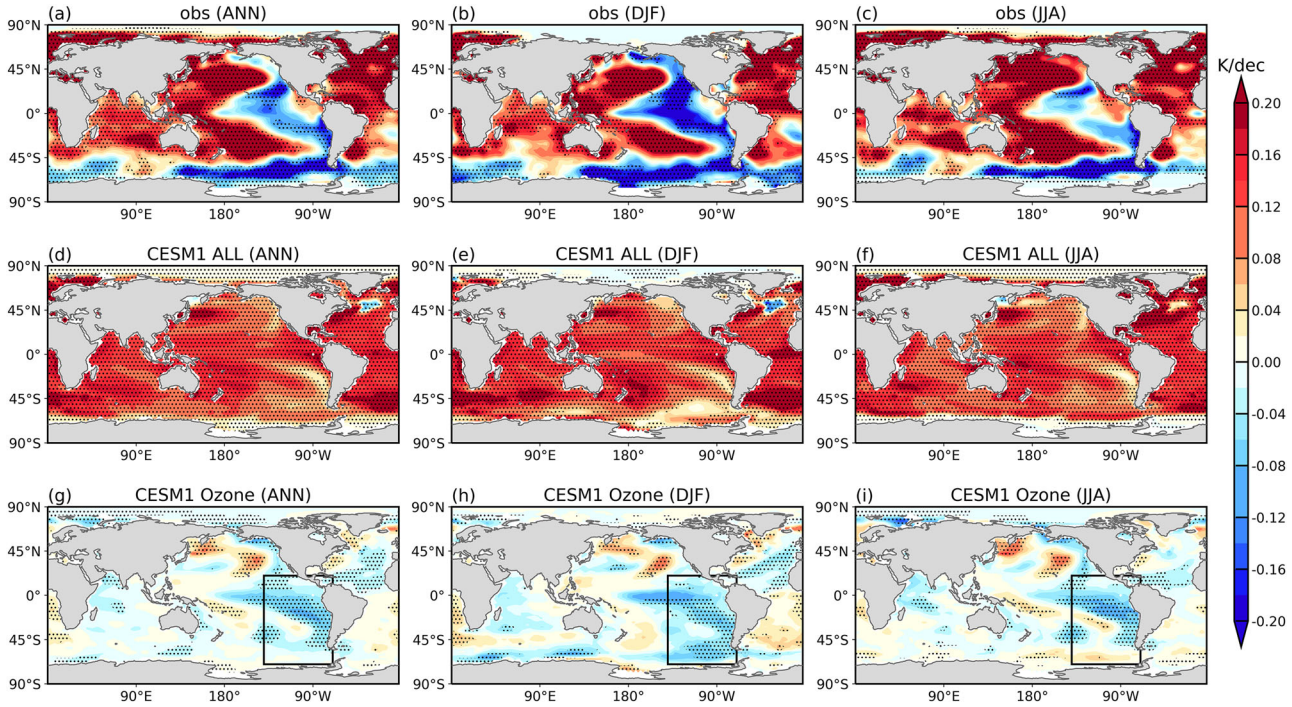

Fig. 1 | Observed and simulated global SST trend patterns during 1980–2014. a–c ERSSTv5 observation; **d–f** CESM1 ALL ensemble mean taken from CESM1 LENS; **g–i** CESM1 simulated response to stratospheric ozone depletion (ALL minus xO3S ensemble mean). From left to right columns are annual-mean, DJF and JJA seasonal means. Stippling indicates where the linear trends are statistically significant at the 95% confidence level. Box in the bottom panels refers to the eastern Pacific area considered for zonal-mean analysis in Fig. 4, defined between 220°E and 290°E, 20°N and 80°S.

tropical cooling trend has only emerged since the 1980s, while stratospheric ozone depletion began in the 1960s and stopped in the 2000s owing to the Montreal Protocol[29]. As a result, the observed SAM increased over the second half of the 20th century but has stopped since the 2000s[30,31], leaving it unclear how the ozone-driven SAM trend would have caused the delayed tropical cooling trend. Second, it is well established that stratospheric ozone depletion drives the positive SAM trend only in austral summer (DJF)[32,33]; yet the observed tropical and SO cooling are present across all seasons (Fig. 1a–c). Further understanding is thus needed to link the highly seasonal signatures of the ozone hole with the annually persistent observed SST trends. Third, most proposed theories have focused mainly on atmospheric pathways (e.g., surface mean-wind advection and cloud feedback[18,21]), it remains unclear how oceanic adjustments in the SO, if any, contribute to the remote tropical response.

Addressing these questions and understanding the mechanisms of remote impacts of the ozone hole requires new modeling experiments to unequivocally isolate the effect of stratospheric ozone depletion. In this study, we accomplish this by using two ensembles with the fully-coupled Community Earth System Model version 1 (CESM1). The first one, denoted "ALL", comprises 20 members taken from the CESM1 Large Ensemble Project[34], integrated with the same historical forcings for 1955–2005 and RCP8.5 forcing for 2006–2020. The second one, denoted "xO3S", is a new 20-member ensemble performed in this study. These simulations are identical to "ALL" except for stratospheric ozone concentrations, which are held fixed at 1955 levels (before the advent of ozone depletion), such that no ozone hole forms in the late 20th Century (see Methods). Although we fix *global* stratospheric ozone, historical changes in stratospheric ozone are the largest over the South Pole and in the austral spring months when the Antarctic ozone hole forms (Fig. S1). Contrasting the ensemble means of these two sets of experiments thus enables us to unequivocally isolate the forced response to stratospheric ozone depletion alone, which we refer to as "OZONE" = "ALL" – "xO3S" in the rest of the paper.

Results

Remote tropical response to stratospheric ozone depletion

We start by showing CESM1 ensemble-mean global SST trend patterns during the recent decades 1980–2014. The ALL ensemble (Fig. 1d–f), like all other CMIP models[1], simulates broad warming trends and fails to reproduce the observed cooling trends in the tropical EP and the SO. On the contrary, a cooling trend response arises from stratospheric ozone depletion (Fig. 1g–i, ALL – xO3S) and is most significant in the tropical and subtropical EP, bearing a considerable resemblance to the observed SST trend pattern. This La Niña-like tropical SST response pattern is further accompanied by a strengthened tropical zonal gradient in sea-level pressure (SLP) and southeasterly trade winds (Fig. S2), which occur in all seasons consistent with observations.

To further illustrate the robust tropical response to stratospheric ozone depletion, we show the 1980–2014 trends in the tropical SST zonal gradient and the Pacific Walker Circulation (PWC) index in all individual members in ALL and xO3S ensembles and observations (Fig. 2). As expected, observations suggest a La Niña-like tropical SST trend pattern and an enhanced PWC trend, while the vast majority of the ALL ensemble members produce a much weaker or even opposite SST and SLP gradient, with only one member resembling the observed SST. More importantly, model biases are even larger in the xO3S ensemble, meaning that the simulated tropical climate would have trended even more toward an El Niño-like SST pattern and a weaker PWC, if stratospheric ozone depletion had not occurred. The ensemble means of tropical SST zonal gradient and the PWC index between the ALL and xO3S ensembles are significantly different, supporting the robust La Niña-like tropical response to stratospheric ozone depletion.

The SST trend pattern (Fig. 1) and the tropical zonal gradients (Fig. 2) confirm a remote impact of stratospheric ozone depletion on the tropics over recent decades in our model. However, unlike in the mechanism hypothesized by the previous study[23], the annual-mean tropical cooling response is not accompanied by a significant SO cooling trend, which only occurs weakly in the southeast Pacific sector in DJF (Fig. 1h). Hence,

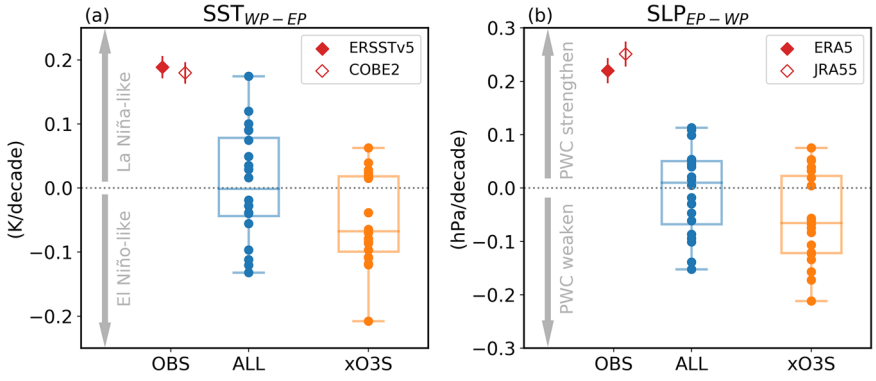

Fig. 2 | Simulated and observed tropical zonal gradient. a Tropical zonal SST gradient (West minus East); **b** tropical zonal sea-level pressure gradient (East minus West, see "Methods"). Blue and orange dots denote all 20 members from ALL (all transient historical forcing) and xO3S (no ozone hole) ensembles, respectively. Red markers denote SST observations and atmospheric reanalysis data ("Methods").

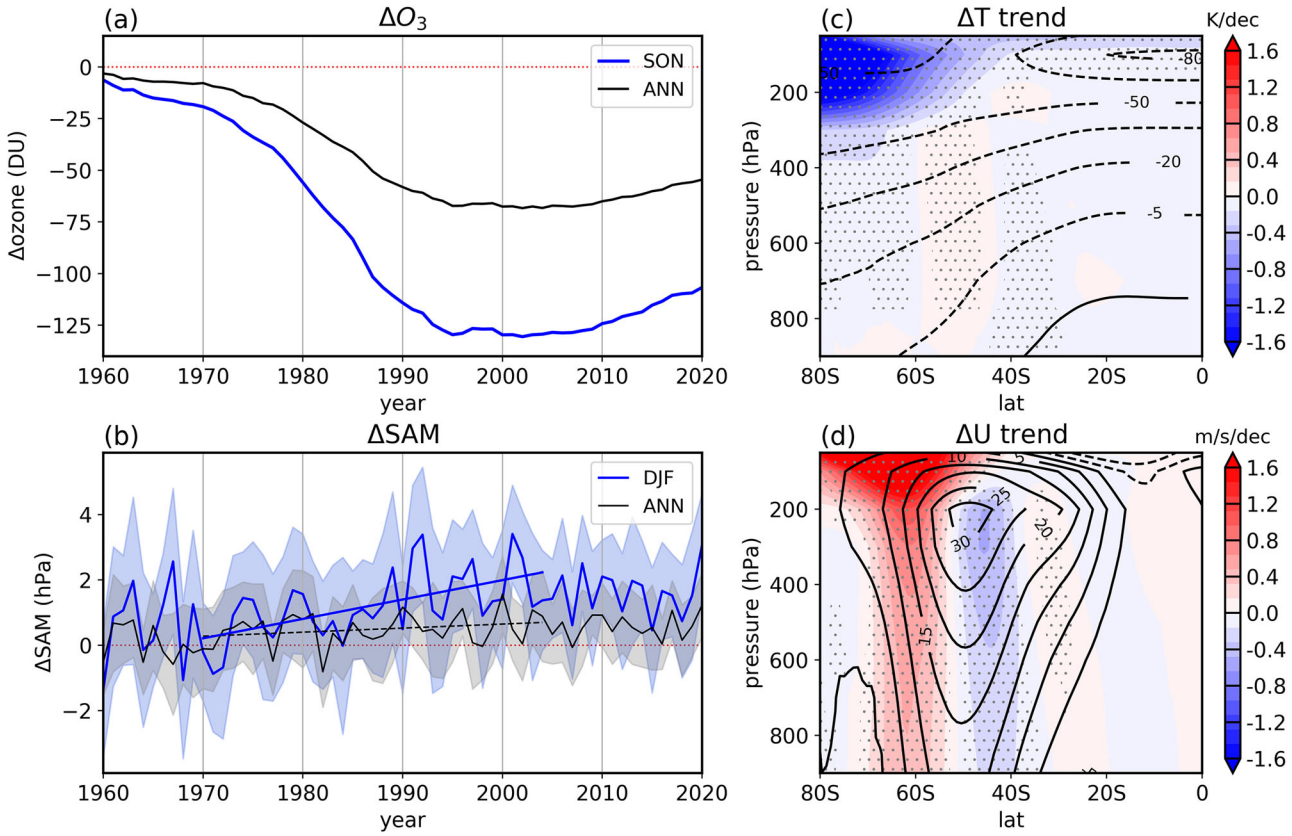

Fig. 3 | Imposed ozone forcing and simulated SH extratropical atmospheric response. a Timeseries of column-integrated stratospheric ozone concentration anomalies southward of 60°S between ALL and xO3S. Blue denotes SON seasonal mean and black denotes annual mean. **b** Timeseries of the simulated SAM response to ozone depletion. Blue denotes DJF seasonal mean and black denotes annual mean. Colored shading represents 0.5 standard deviation across all ensemble members. Colored straight lines denote the linear regression over 1970–2004, with the solid line (blue) for a statistically significant trend in DJF SAM and the dashed line (black) for a statistically insignificant trend in annual mean SAM. **c** Simulated DJF zonal-mean atmospheric temperature trend response and (**d**) DJF zonal-mean atmospheric zonal wind trend response during 1970–2004 to ozone depletion. In (**c**, **d**), black contours are DJF climatological mean levels, stippling indicates where the linear trends are statistically significant at the 95% confidence level.

focusing now on the response to stratospheric ozone alone, we ask: How does the tropical surface cooling from stratospheric ozone depletion come about? Are there changes in the SO involved in – and crucial to – the ozone-driven teleconnections, as previously proposed?

Southern Hemisphere extratropical response to stratospheric ozone depletion

We start by considering the SH atmospheric responses to stratospheric ozone depletion in our simulations. Following the development of the Antarctic ozone hole (Fig. 3a)—most dramatically between the 1970s and the 2000s—we see a significant stratospheric cooling trend over the South Pole, which is largest in the austral summer DJF (Fig. 3c), following the season of the largest ozone loss (blue line in Fig. 3a). This cooling is due to the reduced absorption of ultraviolet solar radiation by stratospheric ozone. The resulting atmospheric temperature anomalies cause a poleward shift in the SH mid-latitude jet (which is largest in DJF, Fig. 3d). While a detailed mechanism remains elusive, the lag between the ozone hole and the jet response is well established in observations[25,35] and robustly simulated in models[27,28,36]. At the surface, the strengthening and pole-ward shift of the westerlies is characterized by the positive phase of the SAM[35] and, as one expects, the SAM trends are only significant in DJF[33] (Fig. 3b).

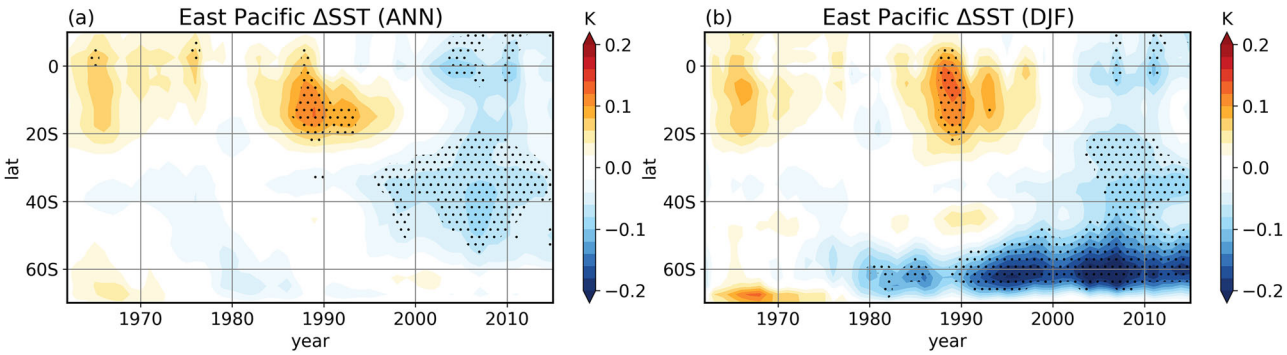

Fig. 4 | Hovmöller diagram of the simulated eastern Pacific SST response to ozone depletion. a Annual-mean SST response; **b** DJF mean SST response. In both panels, SSTs have been low-pass filtered and averaged over the eastern Pacific (box in Fig. 1). Stippling indicates where the ensemble-mean response is statistically significant (see "Methods").

Accompanying the positive SAM trend and enhanced surface westerlies around Antarctica, the SO SSTs also exhibit highly seasonal responses to ozone depletion. During 1970–2004 (the maximum ozone depletion period, Fig. 3a) in DJF, the ozone hole, likely via the positive SAM trends[37], yields a significant SST cooling response in the Pacific and Indian Ocean basins and a warming response in the Atlantic basin (Fig. S3b); in JJA, SST warms in most of the basins (Fig. S3c). As a result, the annual-mean SST trend response is mostly insignificant and weak around Antarctica. The patterns and seasonality of the SO SST response also hold for the more recent decades 1980–2014 (Fig. 1g–i). These results are consistent with recent observational studies[38,39]: although the observed positive SAM trend can produce some SO cooling and Antarctic sea-ice expansion, this SAM-associated SO SST and sea-ice trends are confined to DJF and much weaker than observations. These results imply a limited role of ozone depletion in *fully* explaining the observed SO cooling trends. Other proposed candidates, such as SO natural variability[40,41], freshwater input from Antarctic ice-sheet melting[42,43], or remote influence from tropical Pacific decadal variability[44,45], thus warrant further investigation to understand the observed trends around Antarctica.

In summary, our model simulates the expected DJF tropospheric and surface responses to ozone depletion in the SH extratropics. These include the positive SAM trend associated with the shift in mid-latitude jet and the corresponding SO SST cooling pronounced in the Pacific basin. Turning to the remote tropical response, the key question thus becomes: does the tropical SST response (Fig. 1) in the model result from the ozone-induced SH extratropical changes? If so, does it arise from the regional and seasonal SO SST cooling anomalies as previously proposed, or are there any other mechanisms that might cause the tropical response?

Potential pathways connecting the Southern Ocean and the tropical Pacific

First, to examine how the tropical EP cooling response develops, we consider a Hovmöller diagram of the SST response to ozone depletion averaged over the eastern Pacific basin (see box in Fig. 1 and Methods). A 15-year running average is applied to isolate the low-frequency (decadal to multidecadal) SST response from potential high-frequency variabilities. Focusing on the eastern Pacific allows us to capture the maximum cooling response in both the SO and the tropical Pacific shown in the trend maps (Fig. 1).

Starting from the annual-mean (Fig. 4a), the Hovmöller diagram shows no evidence of a connection between the tropical and SO SST response, as there is no robust SST response in the SO on the annual mean. Yet, significant cooling emerges in the subtropical eastern Pacific in the late 1990s, consistent with the trend map over recent decades (Fig. 1g). Turning to DJF, however, the Hovmöller diagram (Fig. 4b) reveals an interesting communication of cold SST anomalies from the SO to lower latitudes. The SO (in the eastern Pacific basin) experiences cooling throughout the second half of the 20th century, starting from the 1970s along with the onset of the ozone hole. The negative SST anomalies are mostly confined to the high latitudes until the 1990s; after that, the SO SST anomalies expand to lower latitudes, driving a maximum cooling trend in the subtropical and tropical EP between the 1990s and the 2010s. This time-evolving response thus suggests that the tropical cooling response could be in part initiated by the SO changes in DJF. Once the SST cooling anomalies reach the subtropics in the late 1990s, they appear in all seasons and therefore stay in the annual mean (c.f. Fig. 4a, b), suggesting that there are other local processes further amplify the subtropical cooling initiated from the high latitudes.

To further understand the processes contributing to the significant annual-mean subtropical cooling, we perform a mixed-layer heat budget analysis (see Methods) for the SST trends over recent decades (1980–2014, as in Fig. 1), following previous studies[17,19,20]. The heat budget analysis shows that latent heat flux driven by surface wind changes in the central and eastern Pacific (Fig. 5b) and shortwave radiative flux off the coast of South America (Fig. 5c) are the two leading contributors to the simulated subtropical EP cooling response (Fig. 5a). The wind-driven latent heat term represents a coupled mechanism, where increases in surface wind stress cause surface cooling via evaporation, posing an anomalous SST meridional gradient that is conducive to further strengthening surface winds and amplifies surface cooling—the process known as the wind-evaporation-SST (WES) feedback[46]. The shortwave radiative flux term reflects subtropical low-cloud feedback, where surface cooling in the eastern Pacific atmospheric subsidence regions increases low cloud cover via strengthening lower tropospheric stability[3,4,47]. The increased low-cloud cover enhances the reflection of incoming shortwave radiation, further amplifying surface cooling. Both processes exert strong positive feedback for enhancing the magnitude of the subtropical EP cooling, consistent with other modeling studies[18,19]. Furthermore, these feedbacks are not directly ozone-forced and less season-dependent, thus playing a key role in maintaining the subtropical cooling response in all seasons (Figs. 4a and 5a).

While the WES feedback and subtropical cloud feedback appear to make major contributions to the *magnitude* of the simulated tropical SST response, it remains unclear what sets the *timescale* of the tropical SST cooling response following the onset of the ozone hole. The eastern Pacific SST Hovmöller diagrams (Fig. 4b) show that the tropical SST cooling occurs after the 1990s and is pronounced only after the 2000s, while the SO SST cooling begins decades earlier in about 1970s, following the maximum ozone depletion and its significant surface wind response (Fig. 3). This *delayed* timescale thus suggests that – in addition to the previously established *atmospheric* pathways (e.g., surface mean-wind advection in the southeast Pacific[18,21]) that operate on timescales of several years – *oceanic* pathways are also crucial to the teleconnection in our fully-coupled simulations. Indeed, the surface heat budget analysis (Fig. 5) confirms that oceanic processes, following the WES feedback and cloud feedback, make additional positive contributions to the equatorial and mid-latitude SST cooling trends (Fig. 5d). Our further analysis finds that ocean Ekman advection only explains the tropical part (not shown), implying that the midlatitude oceanic process is likely associated with ocean upwelling.

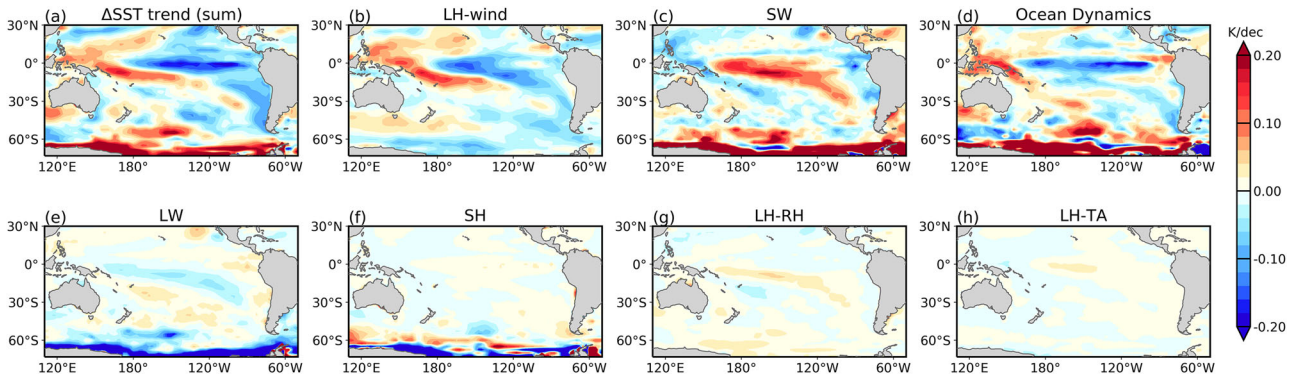

Fig. 5 | Mixed-layer heat budget analysis for the simulated annual-mean Pacific SST trend response to ozone during 1980–2014. a the total SST trend response (sum of all terms, see Methods), the contributions from (**b**) latent heat fluxes due to changes in surface wind speed, **c** shortwave radiation, **d** ocean dynamics, **e** longwave radiation, **f** sensible heat fluxes, **g** latent heat fluxes due to changes in relative humidity and **h** latent heat fluxes due to changes in atmospheric stability.

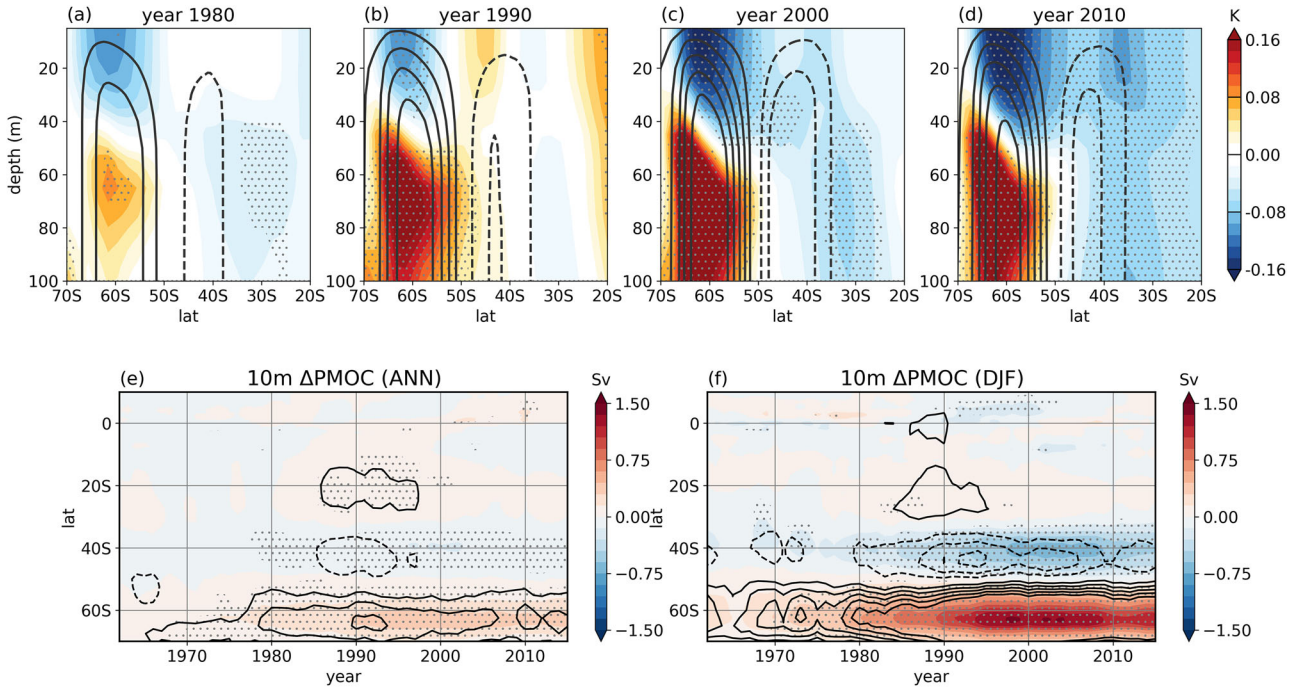

Fig. 6 | Simulated oceanic response (in the Pacific) to ozone depletion. a–d Zonal-mean DJF response of ocean potential temperature (shading) and meridional overturning circulation (contour) in the Pacific basin, averaged over 15-year periods centered in 1980, 1990, 2000, and 2010, respectively. Positive (negative) contours denote clockwise (counterclockwise) MOC responses. Hovmöller diagram of the low-pass filtered (15-yr running averaged) MOC response at 10 m below surface (shading) and surface winds (contour) in the Pacific, in **e** annual mean or **f** DJF. Red (blue) represents positive (negative) MOC response; solid (dashed) contours represent surface westerlies (easterlies).

Although this ocean dynamic contribution is overall smaller in magnitude (Fig. 5d) compared to the other two leading terms, it may shed light on the critical timescale of the communication between high-latitude and low-latitude oceans. Next we will focus on the midlatitude oceanic process and its potential role in the delayed tropical response to ozone depletion.

To examine the oceanic process in midlatitudes, we show four time-slices of 15-year-mean DJF ocean potential temperature and meridional overturning circulation (MOC) response in the Pacific sector, evolving from 1980 to 2010 (Fig. 6a–d). Throughout the period, a positive (clockwise) MOC response is found in the SO centered at 60°S, driven by the anomalous westerlies associated with the positive SAM response (Fig. 6f). This SO MOC consists of northward (cold) advection at the surface causing surface cooling, and upwelling of subsurface warmer waters (Fig. S4) on the polar branch causing subsurface warming[37]. Interestingly, accompanied with this positive MOC response is an opposite MOC response centered around 45°S, which has been reported also in other modeling studies[37,48,49]. This counter-clockwise MOC is driven by the anomalous easterlies in midlatitude arising from the poleward shift of the jet (Fig. 6f). Although this mid-latitude MOC is weaker than the high-latitude MOC, it appears to also affect SST via two distinct stages, similar to the two-time-scale mechanism proposed for the SO MOC[37]. First, on a fast timescale, its surface branch yields surface *warming*, via a poleward Ekman advection from warmer low latitudes to colder high latitudes. Such a warming effect is most evident in the 15-yr average centered in 1990 (note the surface warm blob at 50°S in Fig. 6b). As time evolves, this fast surface wind-driven advection is overwhelmed by an opposite cooling effect, as the slow upwelling becomes more dominant in the second stage (at 40°S). The upwelling branch (at ~40°S) brings colder subsurface water to the surface (Fig. S4), driving slow surface cooling at the equatorward edge after the 2000s (note the surface cooling blob at 40°S in Fig. 6c, d). Once the surface cooling emerges in the mid-latitudes after the

2000s, it propagates to the tropics quickly (Fig. 4b), enhanced by atmospheric positive feedbacks from latent heat changes and shortwave cloud radiative effect (Fig. 5).

In summary: by investigating the surface energy budget and time-evolving ocean response, we find that the remote SST response to ozone depletion results from several processes. The low-latitude SST cooling, occurring decades after the emergence of the SO response, is likely initiated by the midlatitude ocean circulation adjustment, rather than the fast advection of SO SST anomalies as previously proposed. Specifically, the ozone hole causes a poleward shift in midlatitude jet; the resulting surface wind anomalies, consisting of westerlies on the poleward side and easterlies on the equatorward side, drive a dipole pattern of MOC in the Pacific (Fig. 6f). The midlatitude (counter-clockwise) MOC affects SST via two stages: on the fast timescale, southward warm advection associated with easterlies yields midlatitude surface warming (pronounced in ~1990s); on the slow timescale, the equatorward branch of upwelling brings subsurface colder waters to surface, yielding subtropical surface cooling a decade after the onset of the ozone hole (pronounced after 2000s). Although the wind-driven MOC response is stronger in DJF (c.f. Fig. 6e, f), its resulting low-latitude SST changes are persistent in the annual mean, as they are further amplified by other positive feedbacks in the tropics, including the WES feedback and cloud feedback (Fig. 5b, c).

Discussions

In this study, we have provided new modeling evidence that stratospheric ozone depletion can produce remote impacts on tropical oceans, causing SST cooling trends in the tropical East Pacific. Our all-but-stratospheric ozone ("xO3S") experiments unequivocally isolate the surface cooling effect of stratospheric ozone depletion from all other radiative forcing agents. The results imply that stratospheric ozone depletion is a plausible contributor to the formation of the recently observed La Niña-like tropical warming pattern.

The main conclusion of our study broadly confirms the hypothesized impact of the ozone hole on tropical SST trends in ref. 23. However, using specifically designed model simulations, we have been able to elucidate the mechanisms whereby the Antarctic ozone hole causes remote tropical SST cooling trends. Specifically, we emphasize the following points and address the three questions posed at the beginning of this paper:

- The lagged timescales between the ozone hole (maximum between the 1970s and 2000s) and the tropical SST cooling (pronounced over 1980–2015 in observations): While ozone depletion in our model produces a remote impact, the tropical SST response emerges several decades after the onset of the ozone hole in 1970s. This delayed response suggests that oceanic processes play a critical role in initializing the low-latitude SST response. Our results show that midlatitude upwelling is a plausible mechanism, which itself results from ozone-induced surface wind changes.
- The distinct seasonality of the ozone hole and its response: While ozone depletion and its extratropical impacts are limited to austral summer (DJF), the tropical SST response persists across all seasons. This is because atmosphere-ocean coupling in the tropical Pacific provides positive feedbacks (e.g., shortwave cloud feedback and WES feedback) that maintain and enhance the seasonal SST changes.
- The associated atmospheric and oceanic processes: while the simulated magnitude of the subtropical and tropical SST cooling response to ozone is largely determined by shortwave cloud feedback and latent heat flux associated with wind speed changes (the WES feedback), other oceanic processes also make a contribution, particularly the midlatitude upwelling. This ocean circulation response is driven by the shift of midlatitude jets forced by ozone depletion, and appears to be critical in setting the timescale of the teleconnection from high latitudes to low latitudes.

Our findings support the argument that tropical SST patterns could be influenced by remote forcing from the polar regions. Unlike previous modeling studies that used heat flux anomalies to force the SO SST to change[17–20], our simulations employ realistic stratospheric ozone concentrations and allow the atmosphere and oceans to freely respond, providing independent evidence for the teleconnections in the coupled system. Furthermore, while the SH extratropical impact of stratospheric ozone depletion has long been reported, investigations on its remote impact on lower latitudes have been limited to subtropical precipitation[50,51]. Our study establishes a remote impact of stratospheric ozone depletion (mostly over the South Pole) on the tropical oceans, highlighting a novel long-range impact of the ozone hole on tropical and global climate change.

While the goal of our study has been to bring out the specific role of stratospheric ozone depletion, our results in no way exclude the possibility that other processes may also have contributed to the observed tropical Pacific cooling[2]. These may include, and are not limited to, anthropogenic aerosol emissions in the northern hemisphere[12–14], transient response to CO_2 forcing[15], natural variability intrinsic to the Pacific Ocean[10], the Atlantic Ocean[52] or the Southern Ocean[40,41], as well as Antarctic ice-sheet melting[22]. Model biases in tropical SST trend patterns may stem in part from these additional processes. For example, the transient cooling response to CO_2 forcing may be muted due to mode biases in their tropical ocean mean states[15]; additional cooling from Antarctic ice-sheet meltwater is not accounted for in current models, due to the lack of interactive ice-sheet coupling[22,42,43]. Our study suggests that the failure to simulate the observed tropical cooling trends may also be associated with remote response to ozone depletion. Models might underestimate the tropical cooling response to ozone depletion due to their too-weak subtropical low cloud feedback[19] – a common bias in CMIP models[53] – thus biasing their simulated historical trends.

One caveat of this study is that our results are based on a single model. A recent study[54] reported a similar finding using CMIP models, where a La Niña-like SST trend response to ozone is found in CMIP historical ozone-only simulations. Although this provides additional evidence to support our results, we note that those CMIP ozone-only simulations differ from our simulations in several aspects. For example, most CMIP6 models do not have a large ensemble (>10 members) of ozone single-forcing simulations available; some models confound stratospheric and tropospheric ozone, considering the total column of ozone in their simulations. In contrast, our study provides the first set of large-ensemble all-but-stratospheric ozone simulations (to our knowledge) that allow us to robustly separate the forced response to stratospheric ozone depletion. Future confirmation from other models with different physics or different spatial resolutions will be valuable to establish the robustness of our findings.

Finally, and most importantly, we remind the readers that, unlike other GHGs which have continuously increased for many decades and are projected to keep increasing in the coming decades, the Antarctic ozone layer – which was rapidly thinning out in the late 20th century[55] – has started to heal[29] and is projected to recover in the late 21st century as a consequence to the Montreal Protocol[56]. If, as our findings suggest, the ozone hole has indeed been a key driver of the recent La Nina-like tropical SST trends, its closing in the coming decades would contribute to the projected weakening of this trend pattern. It may further drive a reversal towards a more El Niño-like pattern, alongside many other mechanisms that favor this long-time reversal[2]. In that case, the ozone-driven tropical El Niño-like pattern would influence future climate change in an opposite way than the past several decades, including a potentially higher global effective climate sensitivity and more precipitation in the southwestern US. Understanding and quantifying how stratospheric ozone, together with other anthropogenic forcings and natural variability, shape future warming patterns is thus critical for accurately constraining future climate change.

Methods

Model and simulation setup

All simulations analyzed in this study are carried out by the Community Earth System Model (CESM1), with the Community Atmospheric Model version 5 (CAM5), at the 1-degree horizontal resolution. The "ALL"

ensemble, consisting of 20 members, is taken from the CESM1 Large Ensemble project[34]. All ensemble members are forced by the same historical forcings for 1955–2005 and RCP8.5 forcings for 2006–2020, except their initial conditions differ slightly. The "xO3S" ensemble (20 members) is identical to ALL, except their *stratospheric* ozone is held fixed at the 1955 values. This is accomplished as follows: given the vertical distribution of ozone, at each grid box we fix ozone only at levels where its concentration exceeds 150 ppbv[57,58]. This simple procedure avoids having to define a tropopause and leaves tropospheric ozone trends (which cause a substantial radiative forcing and are unrelated to the ozone hole) identical to the one in the historical runs. Note that the large seasonal cycle of stratospheric ozone is retained in the xO3S runs.

Recall that CESM1 has no interactive ozone chemistry, and thus stratospheric ozone and ozone-depleting substances (ODS) are prescribed independently in the model. In the "ALL" and "xO3S" ensembles, ODS concentrations are identical and time-dependent, such that the difference between the two ensembles reflects the impact of stratospheric ozone depletion *alone*, without including the radiative effect of ODS as greenhouse gases, which is large and can cause considerable tropical warming[59,60].

Analysis

The forced response to stratospheric ozone depletion is obtained by taking the ensemble mean difference between ALL and xO3S. Linear trends in any variable of interest are computed using the ordinary least squares (OLS) regression method. The significance of trends is evaluated using the student t-test at the 95% confidence level at each grid box. The significance of responses in Figs. 4 and 6 is evaluated as whether the mean of the response from all 20 ensemble members at each grid box is statistically different from zero at the 95% confidence level.

Indices used for regional analysis

The tropical SST zonal gradient (Fig. 2a) is computed as the difference between SST averaged over 110°E - 180°E, 10°S - 10°N and 210°E - 280°E, 10°S - 10°N (West minus East). A positive (negative) SST gradient refers to a La Niña-like (El Niño-like) SST pattern. The tropical SLP zonal gradient (Fig. 2b), i.e., the Pacific Walker Circulation index[61], is computed as the difference between SLP averaged over 180E - 280°E, 5°S - 5°N and 80°E - 160°E, 5°S - 5°N (East minus West). A positive (negative) SLP gradient refers to a strengthened (weakened) Pacific Walker circulation. The SAM index (Fig. 3b) is computed as the difference between zonal-mean SLP at 45°S and 60°S[26]. The SST Hovmöller diagram (Fig. 4) is computed for SST averaged over the eastern Pacific basin defined as 220°E - 290°E (box in Fig. 1g–i).

Observations

In Fig. 1, we used SST observation from Extended Reconstructed SST data version 5 (ERSSTv5)[62]. In Fig. 2, we used SST observations from ERSSTv5 and the COBE SST dataset[63], and SLP observations from the ERA5[64] and JRA-55[65] reanalysis data. In Fig. S2, we used SLP and 850hPa winds from ERA5[64] reanalysis data.

Mixed-layer heat budget analysis

We perform a mixed-layer heat budget analysis to decompose the contributions to SST trends, following the method widely used in previous studies[17,19,20,66]. We consider the surface energy budget as:

$$\rho C_p H \frac{\partial T}{\partial t} = SW' + LW' + LH' + SH' + OD' \quad (1)$$

where the left hand side represents the mixed-layer heat storage, with ρ being the density of ocean, C_p the specific heat of the ocean, H the ocean mixed-layer depth and T is sea surface temperature. The right hand side represents the mixed-layer heat budget terms, with SW surface shortwave flux, LW surface longwave flux, LH latent heat flux, SH sensible heat flux, and OD ocean heat transport convergence due to ocean dynamics (all heat fluxes are defined as positive downward). $'$ represents the trend between 1980–2014. At the multi-decadal timescale that we consider in this study, the left hand side (the tendency term) is close to zero. Based on the linearized bulk formula for evaporation, latent heat changes associated with Newtonian cooling can be formulized as $\alpha\overline{LH}T'$, where $\alpha \equiv \frac{L_v}{R_v T^2} \approx 0.06/K$, L_v is the latent heat of vaporization, R_v is the gas constant for moist air, $\overline{LH}$ is the climatological mean LH. Such that Eq. 1 can be rewritten into a *diagnostic* equation for the SST trend:

$$T' = -\frac{SW' + LW' + LH'_W + LH'_{RH} + LH'_{\Delta T} + SH' + OD'}{\alpha\overline{LH}} \quad (2)$$

where LH'_W, LH'_{RH}, $LH'_{\Delta T}$ represent latent heat trend changes due to changes in surface wind speed (W), changes in surface relative humidity (RH_0) and changes in air-sea temperature gradient ($\Delta T = T_a - T_s$ with T_a being surface air temperature and T_s surface skin temperature), respectively:

$$LH'_W = \overline{LH}\frac{W'}{\overline{W}} \quad (3)$$

$$LH'_{RH} = -\frac{\overline{LH}RH'_0}{e^{\alpha\overline{\Delta T}} - \overline{RH_0}} \quad (4)$$

$$LH'_{\Delta T} = \frac{\alpha\overline{LH}\,\overline{RH}_0\,\Delta T'}{e^{\alpha\overline{\Delta T}} - \overline{RH_0}} \quad (5)$$

Overbar denotes the climatological mean values.

Data availability

The "ALL" ensemble is taken from the CESM1 LENS project[33], available at https://www.cesm.ucar.edu/community-projects/lens/data-sets. The "xO3S" dataset is available upon request from the corresponding author. ERSSTv5[30] and COBE4[8] SST observations are available from NOAA PSL at https://psl.noaa.gov/data/gridded/data.noaa.ersst.v5.html and https://psl.noaa.gov/data/gridded/data.cobe2.html, respectively. ERA5[49] SLP data is available from the Copernicus Climate Data Store at https://cds.climate.copernicus.eu/#!/search?text=ERA5%20monthly%20single%20levels%26type%3Ddataset. JRA55[50] SLP data is obtained from the NCAR Data Archive at https://rda.ucar.edu/datasets/d628001/.

Code availability

The Python code used to generate figures is available upon request from the corresponding author.

Received: 11 September 2024; Accepted: 22 March 2025;
Published online: 22 April 2025

References

1. Wills, R. C., Dong, Y., Proistosecu, C., Armour, K. C. & Battisti, D. S. Systematic climate model biases in the large-scale patterns of recent sea-surface temperature and sea-level pressure change. *Geophys. Res. Lett.* **49**, e2022GL100011 (2022).
2. Watanabe, M. et al. Possible shift in controls of the tropical Pacific surface warming pattern. *Nature* **630**, 315–324 (2024).
3. Zhou, C., Zelinka, M. D. & Klein, S. A. Impact of decadal cloud variations on the Earth's energy budget. *Nat. Geosci.* **9**, 871–874 (2016).
4. Dong, Y., Proistosescu, C., Armour, K. C. & Battisti, D. S. Attributing historical and future evolution of radiative feedbacks to regional warming patterns using a Green's function approach: the preeminence of the western Pacific. *J. Clim.* **32**, 5471–5491 (2019).
5. England, M. H. et al. Recent intensification of wind-driven circulation in the Pacific and the ongoing warming hiatus. *Nat. Clim. change* **4**, 222–227 (2014).

6. Watanabe, M., Iwakiri, T., Dong, Y. & Kang, S. M. Two competing drivers of the recent Walker circulation trend. *Geophys. Res. Lett.* **50**, e2023GL105332 (2023).
7. Seager, R. et al. Causes of the 2011–14 California drought. *J. Clim.* **28**, 6997–7024 (2015).
8. Kuo, Y. N., Kim, H. & Lehner, F. Anthropogenic aerosols contribute to the recent decline in precipitation over the US Southwest. *Geophys. Res. Lett.* **50**, e2023GL105389 (2023).
9. Lee, S. et al. On the future zonal contrasts of equatorial Pacific climate: perspectives from observations, simulations, and theories. *Npj Clim. Atmos. Sci.* **5**, 82 (2022).
10. Watanabe, M., Dufresne, J. L., Kosaka, Y., Mauritsen, T. & Tatebe, H. Enhanced warming constrained by past trends in equatorial Pacific sea surface temperature gradient. *Nat. Clim. Change* **11**, 33–37 (2021).
11. Rugenstein, M. et al. Connecting the SST pattern problem and the hot model problem. *Geophys. Res. Lett.* **50**, e2023GL105488 (2023).
12. Takahashi, C. & Watanabe, M. Pacific trade winds accelerated by aerosol forcing over the past two decades. *Nat. Clim. Change* **6**, 768–772 (2016).
13. Smith, D. M. et al. Role of volcanic and anthropogenic aerosols in the recent global surface warming slowdown. *Nat. Clim. Change* **6**, 936–940 (2016).
14. Hwang, Y. T., Xie, S. P., Chen, P. J., Tseng, H. Y. & Deser, C. Contribution of anthropogenic aerosols to persistent La Niña-like conditions in the early 21st century. *Proc. Natl. Acad. Sci. USA* **121**, e2315124121 (2024).
15. Seager, R. et al. Strengthening tropical Pacific zonal sea surface temperature gradient consistent with rising greenhouse gases. *Nat. Clim. Change* **9**, 517–522 (2019).
16. Clement, A. C., Seager, R., Cane, M. A. & Zebiak, S. E. An ocean dynamical thermostat. *J. Clim.* **9**, 2190–2196 (1996).
17. Hwang, Y. T., Xie, S. P., Deser, C. & Kang, S. M. Connecting tropical climate change with Southern Ocean heat uptake. *Geophys. Res. Lett.* **44**, 9449–9457 (2017).
18. Kim, H., Kang, S. M., Kay, J. E. & Xie, S. P. Subtropical clouds key to Southern Ocean teleconnections to the tropical Pacific. *Proc. Natl. Acad. Sci. USA* **119**, e2200514119 (2022).
19. Kang, S. M. et al. Global impacts of recent Southern Ocean cooling. *Proc. Natl. Acad. Sci. USA* **120**, e2300881120 (2023).
20. Zhang, X. & Deser, C. Tropical and Antarctic sea ice impacts of observed Southern Ocean warming and cooling trends since 1949. *npj Clim. Atmos. Sci.* **7**, 197 (2024).
21. Dong, Y., Armour, K. C., Battisti, D. S. & Blanchard-Wrigglesworth, E. Two-way teleconnections between the Southern Ocean and the tropical Pacific via a dynamic feedback. *J. Clim.* **35**, 6267–6282 (2022).
22. Dong, Y., Pauling, A. G., Sadai, S. & Armour, K. C. Antarctic ice-sheet meltwater reduces transient warming and climate sensitivity through the sea-surface temperature pattern effect. *Geophys. Res. Lett.* **49**, e2022GL101249 (2022).
23. Hartmann, D. L. The Antarctic ozone hole and the pattern effect on climate sensitivity. *Proc. Natl. Acad. Sci. USA* **119**, e2207889119 (2022).
24. Waugh, D. W., Primeau, F., DeVries, T. & Holzer, M. Recent changes in the ventilation of the southern oceans. *Science* **339**, 568–570 (2013).
25. Thompson, D. W. & Solomon, S. Interpretation of recent Southern Hemisphere climate change. *Science* **296**, 895–899 (2002).
26. Marshall, G. J. Trends in the Southern Annular Mode from observations and reanalyses. *J. Clim.* **16**, 4134–4143 (2003).
27. Polvani, L. M., Waugh, D. W., Correa, G. J. & Son, S. W. Stratospheric ozone depletion: the main driver of twentieth-century atmospheric circulation changes in the Southern Hemisphere. *J. Clim.* **24**, 795–812 (2011).
28. Gillett, N. P. & Thompson, D. W. Simulation of recent Southern Hemisphere climate change. *Science* **302**, 273–275 (2003).
29. Solomon, S. et al. Emergence of healing in the Antarctic ozone layer. *Science* **353**, 269–274 (2016).
30. Polvani, L. M., Previdi, M. & Deser, C. Large cancellation, due to ozone recovery, of future Southern Hemisphere atmospheric circulation trends. *Geophys. Res. Lett.* **38**, L04707 (2011).
31. Banerjee, A., Fyfe, J. C., Polvani, L. M., Waugh, D. & Chang, K. L. A pause in Southern Hemisphere circulation trends due to the Montreal Protocol. *Nature* **579**, 544–548 (2020).
32. Swart, N. C. & Fyfe, J. C. The influence of recent Antarctic ice sheet retreat on simulated sea ice area trends. *Geophys. Res. Lett.* **40**, 4328–4332 (2013).
33. Waugh, D. W., Banerjee, A., Fyfe, J. C. & Polvani, L. M. Contrasting recent trends in Southern Hemisphere Westerlies across different ocean basins. *Geophys. Res. Lett.* **47**, e2020GL088890 (2020).
34. Kay, J. E. et al. The Community Earth System Model (CESM) large ensemble project: A community resource for studying climate change in the presence of internal climate variability. *Bull. Am. Meteorol. Soc.* **96**, 1333–1349 (2015).
35. Thompson, D. W. et al. Signatures of the Antarctic ozone hole in Southern Hemisphere surface climate change. *Nat. Geosci.* **4**, 741–749 (2011).
36. Previdi, M. & Polvani, L. M. Climate system response to stratospheric ozone depletion and recovery. *Q. J. R. Meteorol. Soc.* **140**, 2401–2419 (2014).
37. Ferreira, D., Marshall, J., Bitz, C. M., Solomon, S. & Plumb, A. Antarctic Ocean and sea ice response to ozone depletion: a two-time-scale problem. *J. Clim.* **28**, 1206–1226 (2015).
38. Polvani, L. M. et al. Interannual SAM modulation of Antarctic Sea ice extent does not account for its long-term trends, pointing to a limited role for ozone depletion. *Geophys. Res. Lett.* **48**, e2021GL094871 (2021).
39. Dong, Y., Polvani, L. M. & Bonan, D. B. Recent multi-decadal southern ocean surface cooling unlikely caused by southern annular mode trends. *Geophys. Res. Lett.* **50**, e2023GL106142 (2023).
40. Polvani, L. M. & Smith, K. L. Can natural variability explain observed Antarctic sea ice trends? New modeling evidence from CMIP5. *Geophys. Res. Lett.* **40**, 3195–3199 (2013).
41. Zhang, L., Delworth, T. L., Cooke, W. & Yang, X. Natural variability of Southern Ocean convection as a driver of observed climate trends. *Nat. Clim. Change* **9**, 59–65 (2019).
42. Schmidt, G. A. et al. Anomalous meltwater from ice sheets and ice shelves is a historical forcing. *Geophys. Res. Lett.* **50**, e2023GL106530 (2023).
43. Roach, L. A. et al. Winds and meltwater together lead to Southern Ocean surface cooling and sea ice expansion. *Geophys. Res. Lett.* **50**, e2023GL105948 (2023).
44. Meehl, G. A., Arblaster, J. M., Bitz, C. M., Chung, C. T. & Teng, H. Antarctic sea-ice expansion between 2000 and 2014 driven by tropical Pacific decadal climate variability. *Nat. Geosci.* **9**, 590–595 (2016).
45. Chung, E. S. et al. Antarctic sea-ice expansion and Southern Ocean cooling linked to tropical variability. *Nat. Clim. Change* **12**, 461–468 (2022).
46. Xie, S. P. et al. Global warming pattern formation: sea surface temperature and rainfall. *J. Clim.* **23**, 966–986 (2010).
47. Wood, R. & Bretherton, C. S. On the relationship between stratiform low cloud cover and lower-tropospheric stability. *J. Clim.* **19**, 6425–6432 (2006).
48. Bitz, C. M. & Polvani, L. M. Antarctic climate response to stratospheric ozone depletion in a fine resolution ocean climate model. *Geophysl. Res. Lett.* **39**, L20705 (2012).
49. Sigmond, M. & Fyfe, J. C. Has the ozone hole contributed to increased Antarctic sea ice extent?. *Geophys. Res. Lett.* **37**, L18502 (2010).

50. Kang, S. M., Polvani, L. M., Fyfe, J. C. & Sigmond, M. Impact of polar ozone depletion on subtropical precipitation. *Science* **332**, 951–954 (2011).
51. Wu, Y. & Polvani, L. M. Recent trends in extreme precipitation and temperature over southeastern South America: the dominant role of stratospheric ozone depletion in the CESM Large Ensemble. *J. Clim.* **30**, 6433–6441 (2017).
52. McGregor, S., Stuecker, M. F., Kajtar, J. B., England, M. H. & Collins, M. Model tropical Atlantic biases underpin diminished Pacific decadal variability. *Nat. Clim. Change* **8**, 493–498 (2018).
53. Myers, T. A. et al. Observational constraints on low cloud feedback reduce uncertainty of climate sensitivity. *Nat. Clim. Change* **11**, 501–507 (2021).
54. Chung, E. S. et al. Tropical eastern Pacific cooling trend reinforced by human activity. *npj Clim. Atmos. Sci.* **7**, 170 (2024).
55. Farman, J. C., Gardiner, B. G. & Shanklin, J. D. Large losses of total ozone in Antarctica reveal seasonal ClO x/NO x interaction. *Nature* **315**, 207–210 (1985).
56. Dhomse, S. S. et al. Estimates of ozone return dates from Chemistry-Climate Model Initiative simulations. *Atmos. Chem. Phys.* **18**, 8409–8438 (2018).
57. Young, P. J. et al. Pre-industrial to end 21st century projections of tropospheric ozone from the Atmospheric Chemistry and Climate Model Intercomparison Project (ACCMIP). *Atmos. Chem. Phys.* **13**, 2063–2090 (2013).
58. Prather, M. J., Zhu, X., Tang, Q., Hsu, J. & Neu, J. L. An atmospheric chemist in search of the tropopause. *J. Geophys. Res.* **116**, D04306 (2011).
59. Polvani, L. M. & Bellomo, K. The key role of ozone-depleting substances in weakening the walker circulation in the second half of the twentieth century. *J. Clim.* **32**, 1411–1418 (2019).
60. Polvani, L. M., Previdi, M., England, M. R., Chiodo, G. & Smith, K. L. Substantial twentieth-century Arctic warming caused by ozone-depleting substances. *Nat. Clim. Change* **10**, 130–133 (2020).
61. Vecchi, G. A. et al. Weakening of tropical Pacific atmospheric circulation due to anthropogenic forcing. *Nature* **441**, 73–76 (2006).
62. Huang, B. et al. Extended reconstructed sea surface temperature, version 5 (ERSSTv5): upgrades, validations, and intercomparisons. *J. Clim.* **30**, 8179–8205 (2017).
63. Ishii, M., Shouji, A., Sugimoto, S. & Matsumoto, T. Objective analyses of sea-surface temperature and marine meteorological variables for the 20th century using ICOADS and the Kobe collection. *Int. J. Climatol.: A J. R. Meteorol. Soc.* **25**, 865–879 (2005).
64. Hersbach, H. et al. The ERA5 global reanalysis. *Q. J. R. Meteorolo. Soc.* **146**, 1999–2049 (2020).
65. Kobayashi, S. et al. The JRA-55 reanalysis: General specifications and basic characteristics. *J. Meteorol. Soc. Jpn. Ser. II* **93**, 5–48 (2015).
66. Kang, S. M. et al. Walker circulation response to extratropical radiative forcing. *Sci. Adv.* **6**, eabd3021 (2020).

Acknowledgements

Y.D. is supported by the NOAA Climate and Global Change Postdoctoral Fellowship Program, administered by UCAR's Cooperative Programs for the Advancement of Earth System Science (CPAESS) under award NA210AR4310383. L.M.P. is supported, in part, by an award from the US National Science Foundation to Columbia University. Y.T.H. is supported by National Science and Technology Council (NSTC 112-2111-M-002-016-MY4). M.R.E. is supported by Royal Commission for the Exhibition of 1851. We would like to acknowledge high-performance computing support from Cheyenne (https://doi.org/10.5065/D6RX99HX) provided by NCAR's Computational and Information Systems Laboratory, sponsored by the National Science Foundation. Y.T.H. was supported by Ministry of Science and Technology of Taiwan (NSTC 112-2111-M-002-016-MY4).

Author contributions

Y.D. designed and performed the research; M.R.E. and Y.D. conducted the xO3S simulations. Y.D. analyzed data and wrote the initial draft. All authors contributed to the result interpretation and the final draft.

Competing interests

The authors declare no competing interests.

Additional information

Supplementary information The online version contains supplementary material available at https://doi.org/10.1038/s41612-025-01020-0.

Correspondence and requests for materials should be addressed to Yue Dong.